RESEARCH MEMORANDUM

AERODYNAMIC CHARACTERISTICS AT A MACH NUMBER OF 6.8 OF TWO HYPERSONIC MISSILE CONFIGURATIONS, ONE WITH LOW-ASPECT-RATIO CRUCIFORM FINS AND TRAILING-EDGE FLAPS AND ONE WITH A FLARED AFTERBODY AND ALL-MOVABLE CONTROLS

By Ross B. Robinson and Peter T. Bernot

Langley Aeronautical Laboratory
Langley Field, Va.

CLASSIFIED DOCUMENT

NATIONAL ADVISORY COMMITTEE
FOR AERONAUTICS

WASHINGTON

August 4, 1958

NATIONAL ADVISORY COMMITTEE FOR AERONAUTICS

RESEARCH MEMORANDUM

AERODYNAMIC CHARACTERISTICS AT A MACH NUMBER OF 6.8 OF TWO HYPERSONIC MISSILE CONFIGURATIONS, ONE WITH LOW-ASPECT-RATIO CRUCIFORM FINS AND TRAILING-EDGE FLAPS AND ONE WITH A FLARED AFTERBODY AND ALL-MOVABLE CONTROLS*

By Ross B. Robinson and Peter T. Bernot

SUMMARY

An investigation has been made to determine the aerodynamic characteristics in pitch at a Mach number of 6.8 of hypersonic missile configurations with cruciform trailing-edge flaps and with all-movable control surfaces. The flaps were tested on a configuration having low-aspect-ratio cruciform fins with an apex angle of 5°; the all-movable controls were mounted at the 46.7-percent body station on a configuration having a 10° flared afterbody. The tests were made through an angle-of-attack range of -2° to 20° at zero sideslip in the Langley 11-inch hypersonic tunnel.

The results indicated that the all-movable controls on the flared-afterbody model should be capable of producing much larger values of trim lift and of normal acceleration than the trailing-edge-flap configuration. The flared-afterbody configuration had considerably higher drag than the cruciform-fin model but only slightly lower values of lift-drag ratio.

INTRODUCTION

In order to obtain information on stability and control of configurations that offer promise as hypersonic missiles, an investigation of a family of missile models has been undertaken. The initial phases of the investigation are reported in reference 1 for a Mach number of 2.01 and in reference 2 for Mach numbers from 2.29 to 4.65. Included in reference 1 are the results of tests of some canard control surfaces for configurations with a flared afterbody and with cruciform fins.

*Title, Unclassified.

This general investigation has been extended to obtain control information at higher Mach numbers for modified versions of two of the configurations presented in references 1 and 2. These versions consisted of (1) trailing-edge-flap controls on a configuration having low-aspect-ratio cruciform fins and (2) a configuration with a 10° flared afterbody equipped with all-movable cruciform controls. The two configurations were considerably different geometrically but were selected as possible hypersonic missile arrangements from the standpoint of stability, maneuverability, and heating requirements. This report presents the results of an investigation of the aerodynamic characteristics of these control arrangements at a Mach number of 6.8.

COEFFICIENTS AND SYMBOLS

The data are presented as coefficients of forces and moments with the center of moments at 50-percent of the body length. All data are referred to the body-axis system except lift and drag which are referred to the wind-axis system.

C_N	normal-force coefficient, F_N/qS
C_L	lift coefficient, F_L/qS
C_A	axial-force coefficient, F_A/qS
C_D	drag coefficient, F_D/qS
C_Y	side-force coefficient, F_Y/qS
C_l	rolling-moment coefficient, M_X/qSd
C_m	pitching-moment coefficient, M_Y/qSd
C_n	yawing-moment coefficient, M_Z/qSd
F_N	normal force
F_L	lift
F_A	axial force
F_D	drag
F_Y	side force

[redacted]

M_X	rolling moment
M_Y	pitching moment
M_Z	yawing moment
q	free-stream dynamic pressure
S	cross-sectional area of cylindrical section of body
d	diameter of cylindrical section of body
α	angle of attack of body center line, deg
δ_c	deflection of all-movable controls with respect to body center line, positive when trailing edge is down or left, deg
δ_f	deflection of trailing-edge flap with respect to body center line, positive when trailing edge is down or left, deg
L/D	lift-drag ratio, C_L/C_D
x	longitudinal distance rearward of nose, in.
R	radius, in.

MODELS AND APPARATUS

Sketches of the models are shown in figure 1. The geometric characteristics of the models are given in table I, and the coordinates of the forebody are given in table II.

The model had a body consisting of a 5-caliber forebody with a round nose followed by a straight tapered section that fairs into a 5-caliber cylindrical afterbody. The fins, trailing-edge flaps, and all-movable controls were flat plates with rounded leading edges and blunt trailing edges.

The cruciform-fin configuration consisted of the body, cruciform fins having a 5° apex angle, and cruciform trailing-edge flaps in the plane of the fins (fig. 1). An 0.033-caliber gap separated the fins and flaps. The hinge line of the flaps was at the 93.3-percent body station and the 33.3-percent chord line of the flaps.

[redacted]

The flared-afterbody configuration was composed of the body, a 2-caliber 10° flared afterbody, and modified 70° delta cruciform all-movable controls. The control-surface hinge lines were at the 46.7-percent body station and the 68.7-percent-chord line of the controls.

Six-component force and moment data were measured by an internal strain-gage balance. Pressure recorders provided a continuous record of the settling-chamber and model base pressures. (See ref. 3.) The base pressures were measured by a single tube placed in the balance chamber slightly forward of the model base.

The investigation was made in the Langley 11-inch hypersonic tunnel described in reference 4. The tunnel is of the intermittent-flow type employing a single-step, two-dimensional Invar nozzle.

TESTS, CORRECTIONS, AND ACCURACY

The tests were made at a Mach number of 6.8, a stagnation temperature of about 650° F, and a stagnation pressure of 21 atmospheres absolute (310 pounds per square inch). The Reynolds number was approximately 3.1×10^6 based on the body length of one foot. Based on previous experience (see ref. 5), the model boundary layer was believed to be laminar for these test conditions. Test-section temperatures were maintained above values necessary to prevent liquefaction of the air. The dewpoint was below -75° F measured at atmospheric pressure. Tests were made through an angle-of-attack range from -2° to 20° at zero sideslip only.

The Mach number variation during a run was about 0.5 percent and flow angularities were negligible. No corrections have been applied to the data for these variations.

The axial-force data were adjusted to a base pressure equal to the free-stream static pressure. Base pressures measured in the balance chamber were applied to the total base area of the model. The values of base pressure were accurate to within ±2 percent and values of stagnation pressure to within ±1 percent.

Estimated probable errors in the results of the present tests based on balance calibration, zero shifts, and repeatibility are as follows:

C_N and C_L	±0.050
C_A and C_D	±0.007
C_m	±0.040
C_l	±0.009

[redacted]

C_n	±0.019
C_Y	±0.015
α, deg	±0.2
δ_p and δ_c, deg	±0.1

PRESENTATION OF RESULTS

The aerodynamic characteristics in pitch for the various configurations are presented as follows:

	Figure
Body alone	2
Body with 5° fins and trailing-edge flaps	3
Body with 10° flare and all-movable controls	4
Variation of C_m with C_N for trailing-edge flap control and all-movable control configurations	5
Roll control with trailing-edge flaps	6
Roll control with all-movable controls	7

SUMMARY OF RESULTS

The finned configuration with trailing-edge flaps and the flared afterbody configuration with all-movable controls indicate approximately the same level of static longitudinal stability. (See fig. 5.) However, of the two configurations investigated, the all-movable control arrangement is considerably more effective than the trailing-edge-flap arrangement in producing trimmed normal force or normal accelarations.

For zero control deflection, the finned configuration with trailing-edge flaps has a higher maximum lift-drag ratio L/D than the flared afterbody configuration with all-movable controls. (See figs. 3(b) and 4(b).) However, the losses in L/D due to control deflection are greater with the trailing-edge flaps than with the all-movable controls. As a result, even for the most rearward center-of-gravity position permissible to avoid regions of longitudinal instability, the values of trimmed L/D would be about the same for the two configurations.

Both control arrangements, when deflected differentially, provided positive roll effectiveness that increased slightly with increasing angle of attack. With all four trailing-edge flaps deflected differentially,

a favorable yawing moment was produced throughout the angle-of-attack range. With the vertical all-movable controls deflected differentially, an increasingly adverse yawing moment occurred with increasing angle of attack.

Langley Aeronautical Laboratory,
National Advisory Committee for Aeronautics,
Langley Field, Va., April 10, 1958.

REFERENCES

1. Robinson, Ross B.: Wind-Tunnel Investigation at a Mach Number of 2.01 of the Aerodynamic Characteristics in Combined Angles of Attack and Sideslip of Several Hypersonic Missile Configurations With Various Canard Controls. NACA RM L58A21, 1958.

2. Turner, Kenneth L., and Appich, W. H., Jr.: Investigation of the Static Stability Characteristics of Five Hypersonic Missile Configurations at Mach Numbers From 2.29 to 4.65. NACA RM L58D04, 1958.

3. McLellan, Charles H., Williams, Thomas W., and Bertram, Mitchel H.: Investigation of a Two-Step Nozzle in the Langley 11-Inch Hypersonic Tunnel. NACA TN 2171, 1950.

4. McLellan, Charles H., Williams, Thomas W., and Beckwith, Ivan E.: Investigation of the Flow Through a Single-Stage Two-Dimensional Nozzle in the Langley 11-Inch Hypersonic Tunnel. NACA TN 2223, 1950.

5. Becker, John V., and Korycinski, Peter F.: Heat Transfer and Pressure Distribution at a Mach Number of 6.8 on Bodies With Conical Flares and Extensive Flow Separation. NACA RM L56F22, 1956.

TABLE I.- GEOMETRIC CHARACTERISTICS OF MODELS

Body:	
Length, in.	12.00
Diameter, in.	1.20
Cross-sectional area, sq in.	1.13
Length-diameter ratio of nose	5.0
Length-diameter ratio, total	10.0
Moment center location, percent length	50.0
Flare:	
Length, in.	2.40
Base diameter, in.	2.046
Base area, sq in.	3.29
Apex angle, deg	10.0
Fins (Including flaps):	
Area of two panels exposed, sq in.	4.90
Root chord, exposed, in.	7.61
Tip chord, in.	1.20
Span, exposed, in.	1.08
Aspect ratio of exposed fins	2.38
Leading-edge apex angle, deg	5.0
Span-diameter ratio, total	1.90
Trailing-edge flaps:	
Area, per pair, sq in.	1.30
Span, each, in.	0.54
Chord, each, in.	1.20
Percent of fin area	26.5
Leading-edge sweep, deg	0
Hinge line, percent body length	93.3
Hinge line, percent chord	33.3
Gap, in.	0.04
All-movable controls:	
Area, exposed, per pair, sq in.	2.50
Root chord, in.	2.55
Tip chord, in.	0.14
Span, exposed, in.	0.89
Leading-edge sweep, deg	70.0
Hinge line, percent body length	46.7
Hinge line, percent root chord	68.7

[redacted]

TABLE II.- COORDINATES OF FOREBODY

x, in.	R, in.
0	0
.106	.106
2.400	.385
2.800	.429
3.200	.470
3.600	.505
4.000	.534
4.400	.558
4.800	.576
5.200	.590
5.600	.597
6.000	.600

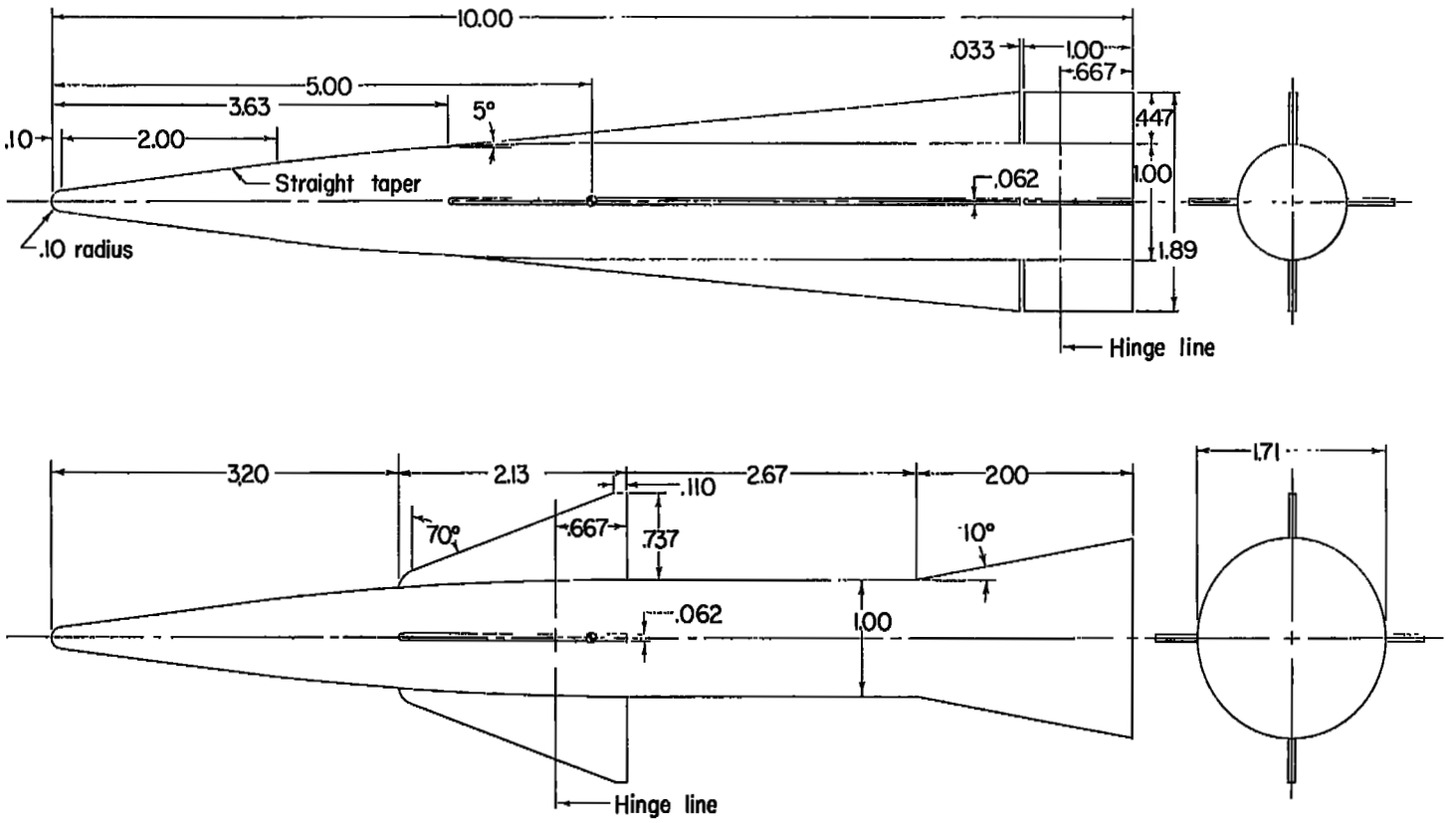

Figure 1.- Details of models. All linear dimensions are in calibers.

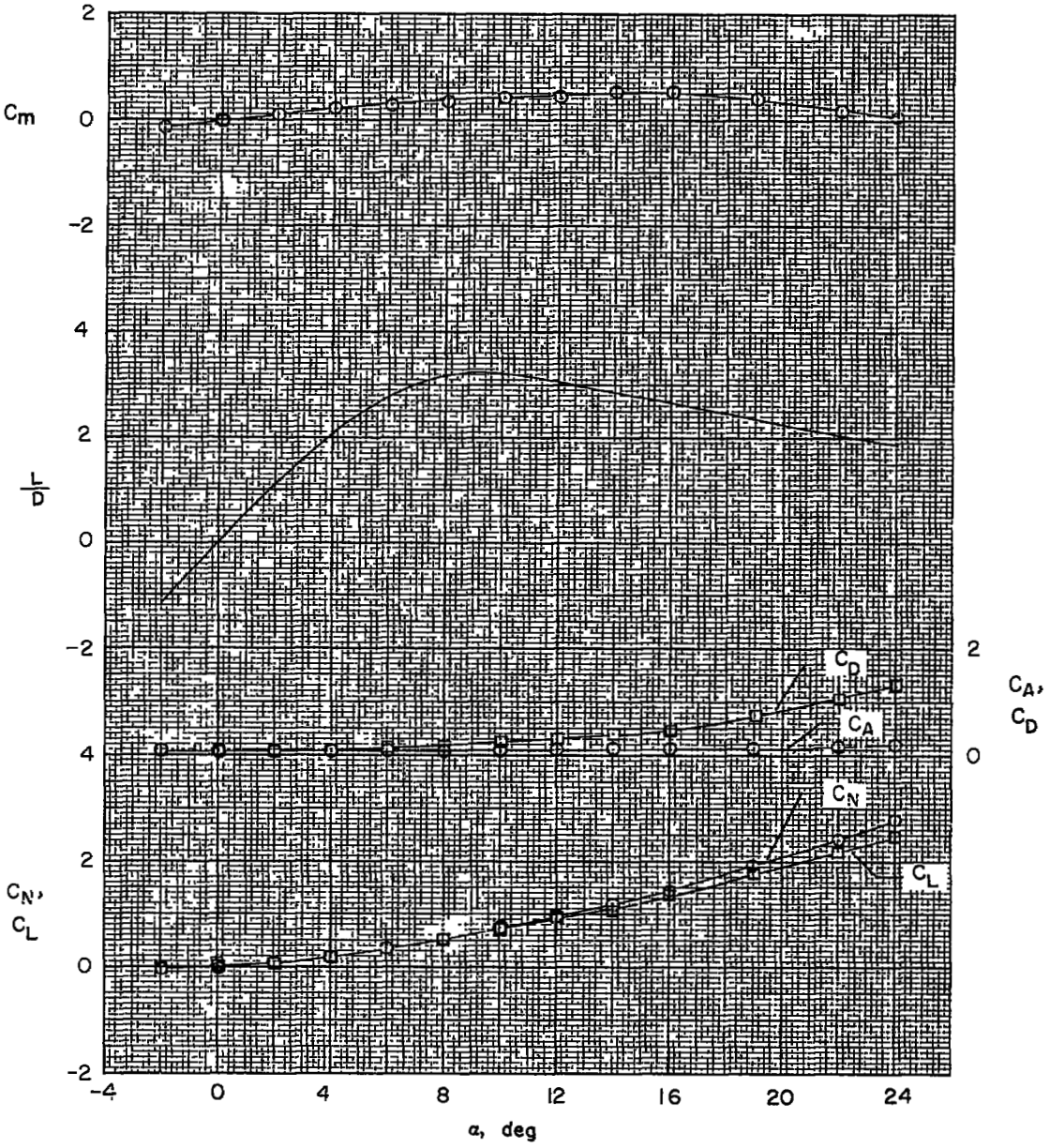

Figure 2.- Aerodynamic characteristics in pitch for body alone.

[redacted]

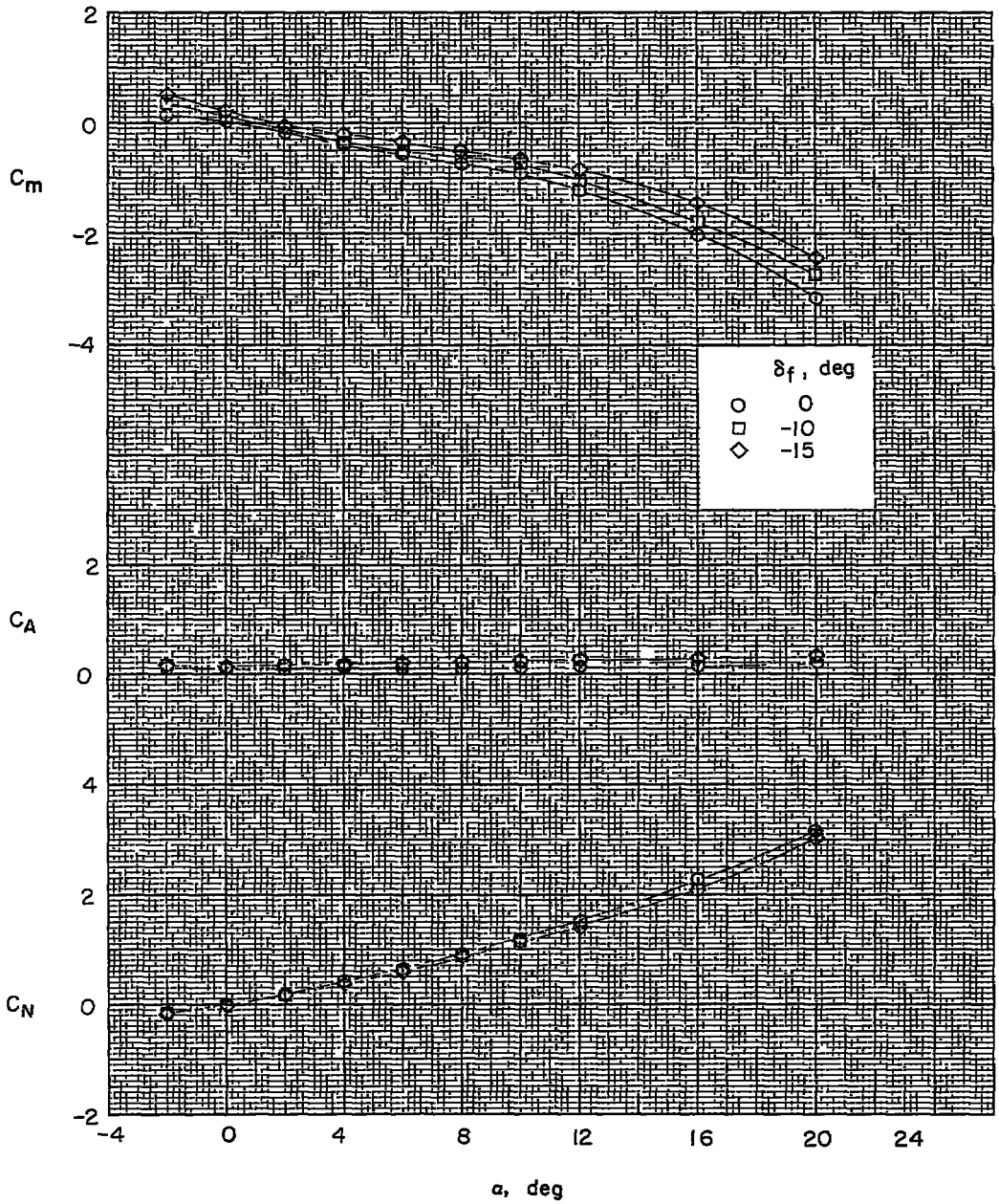

(a) Body axis.

Figure 3.- Effects of control deflection on aerodynamic characteristics in pitch. Body with 5° fins and trailing-edge-flap control.

[redacted]

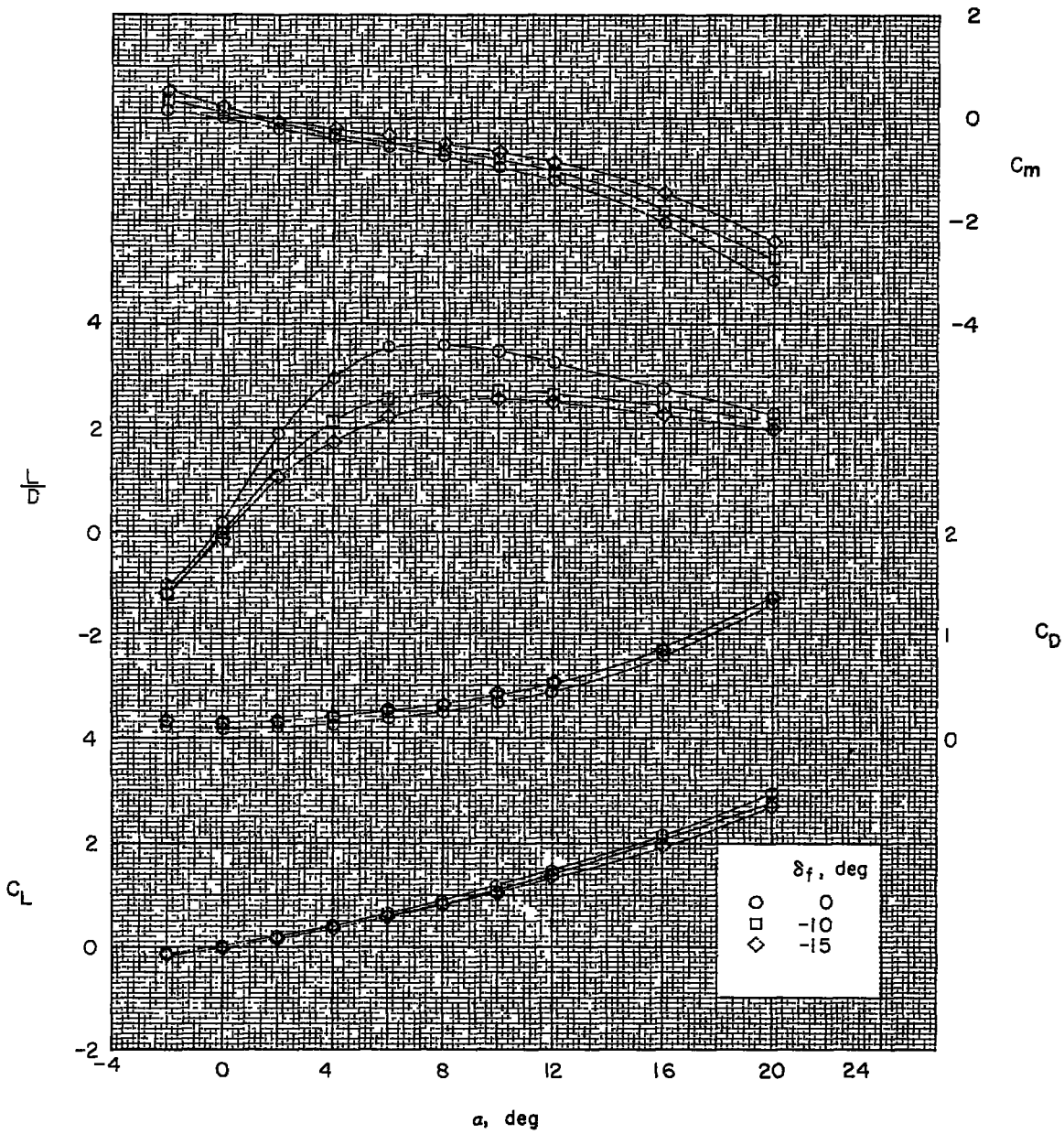

(b) Wind axis.

Figure 3.- Concluded.

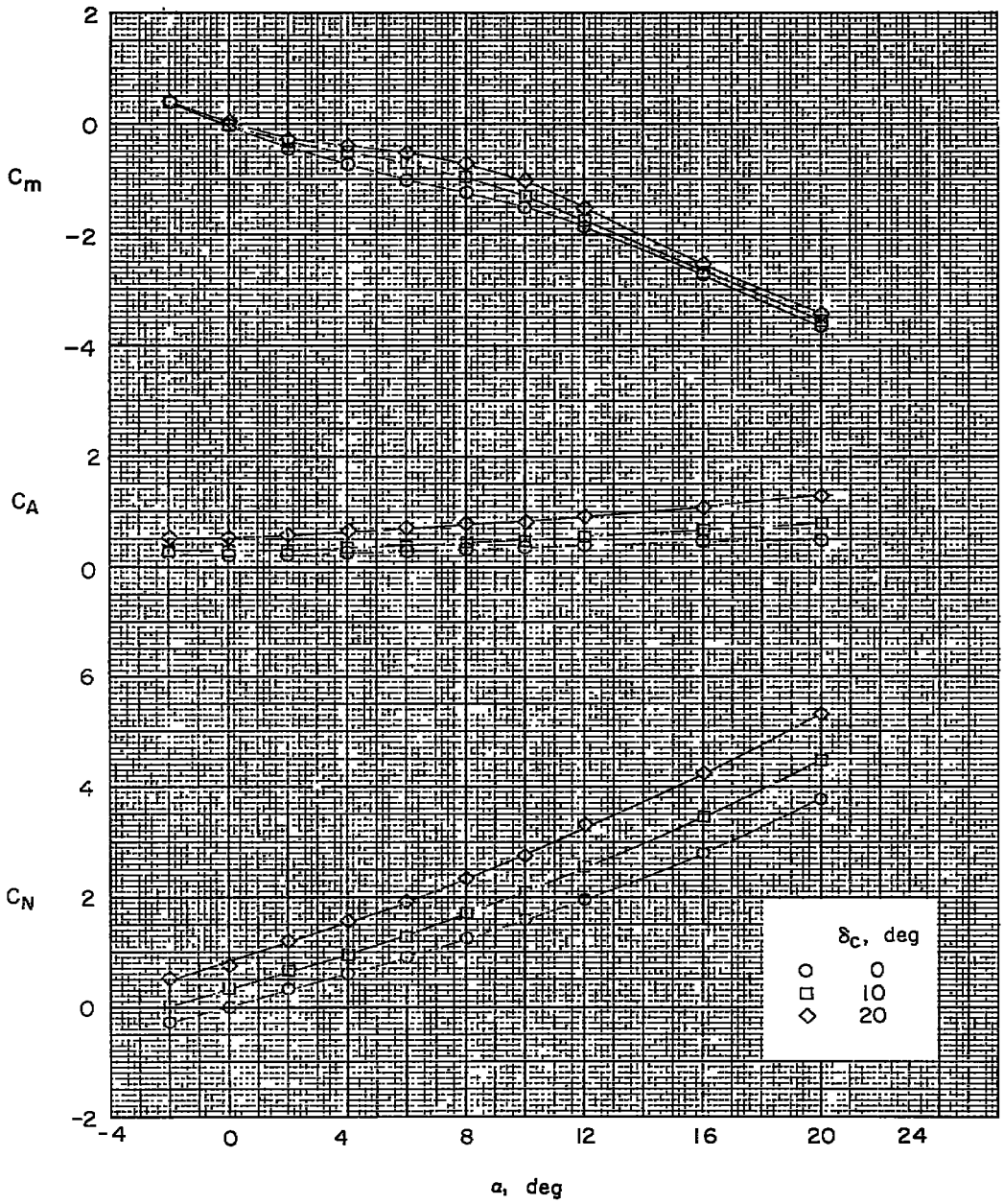

(a) Body axis.

Figure 4.- Effects of control deflection on aerodynamic characteristics in pitch. Body with flare and all-movable control.

[redacted]

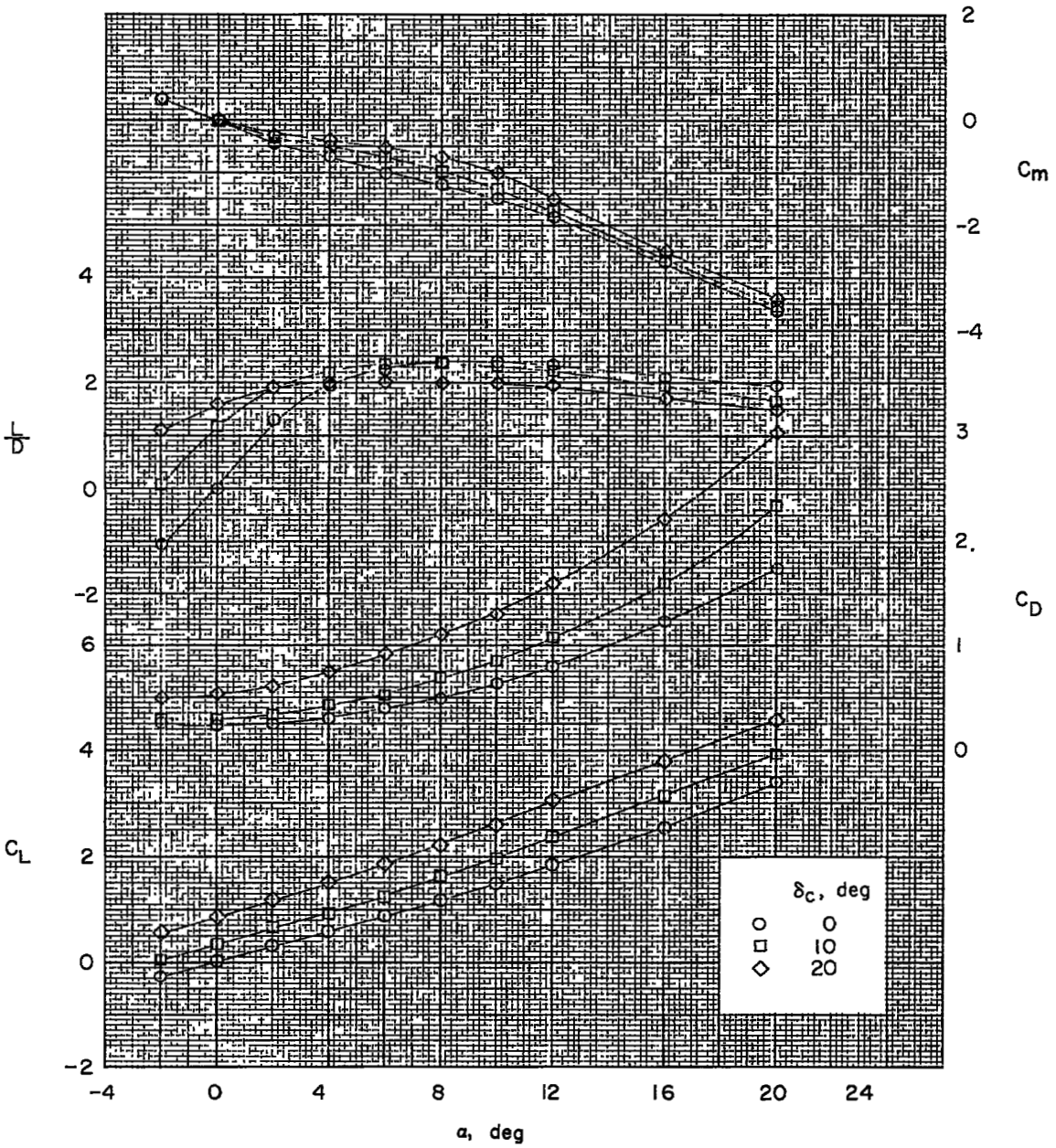

(b) Wind axis.

Figure 4.- Concluded.

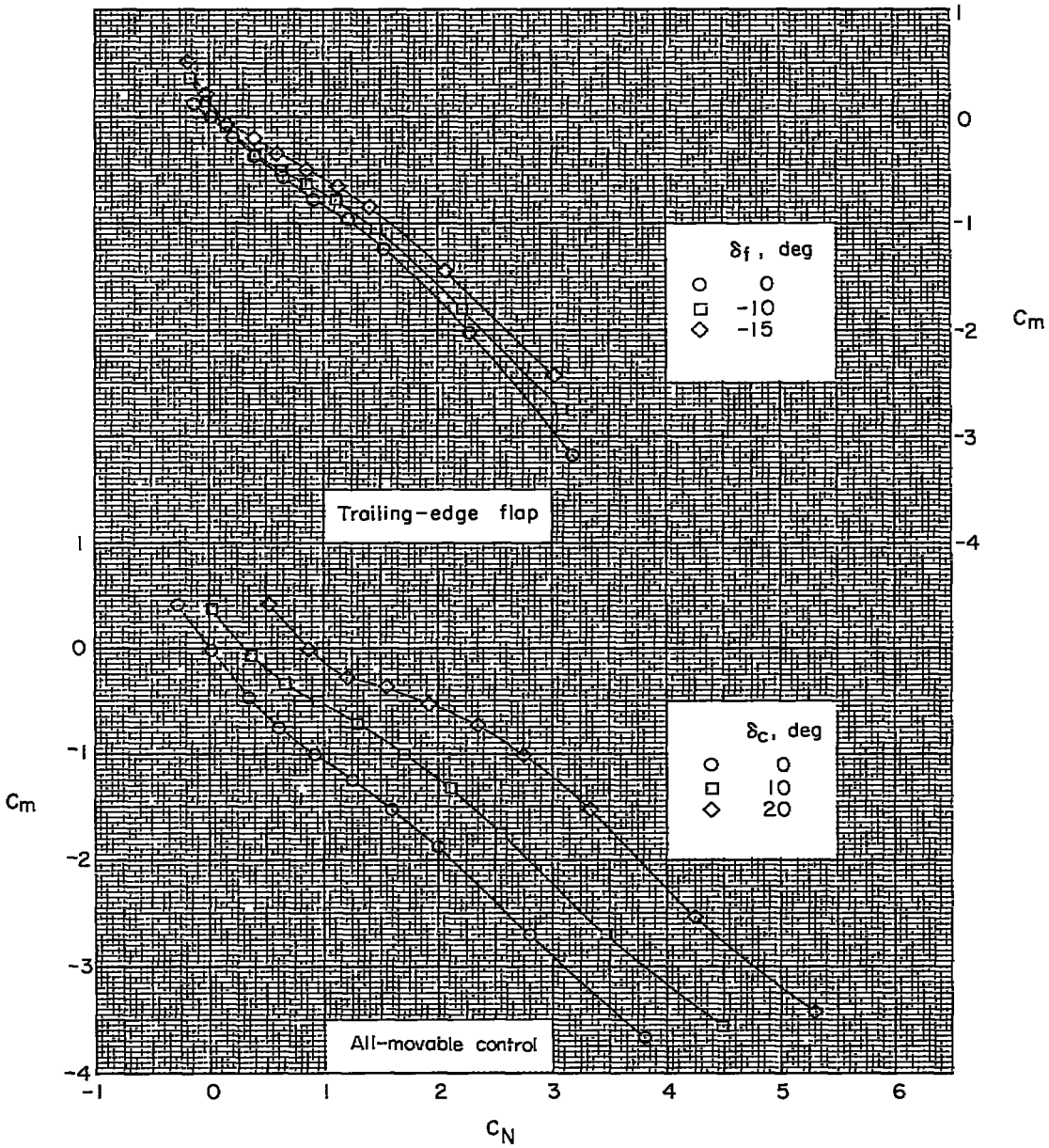

Figure 5.- Effects of control deflection on variation of C_m with C_N.

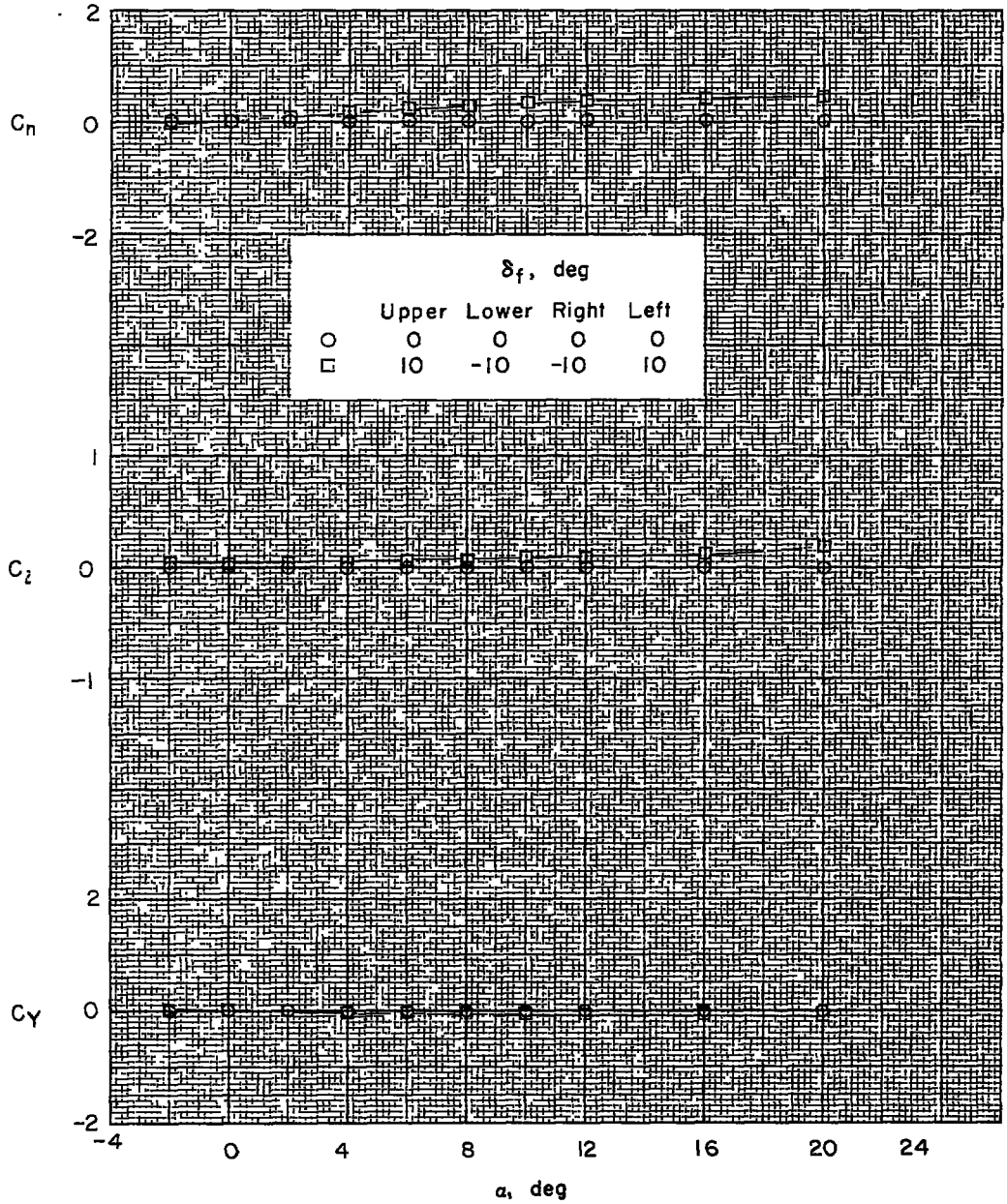

(a) Variation of C_n, C_l, and C_Y with α.

Figure 6.- Effects of differential deflection for roll control. Body with 5° fins and trailing-edge-flap control; body-axis system.

[redacted]

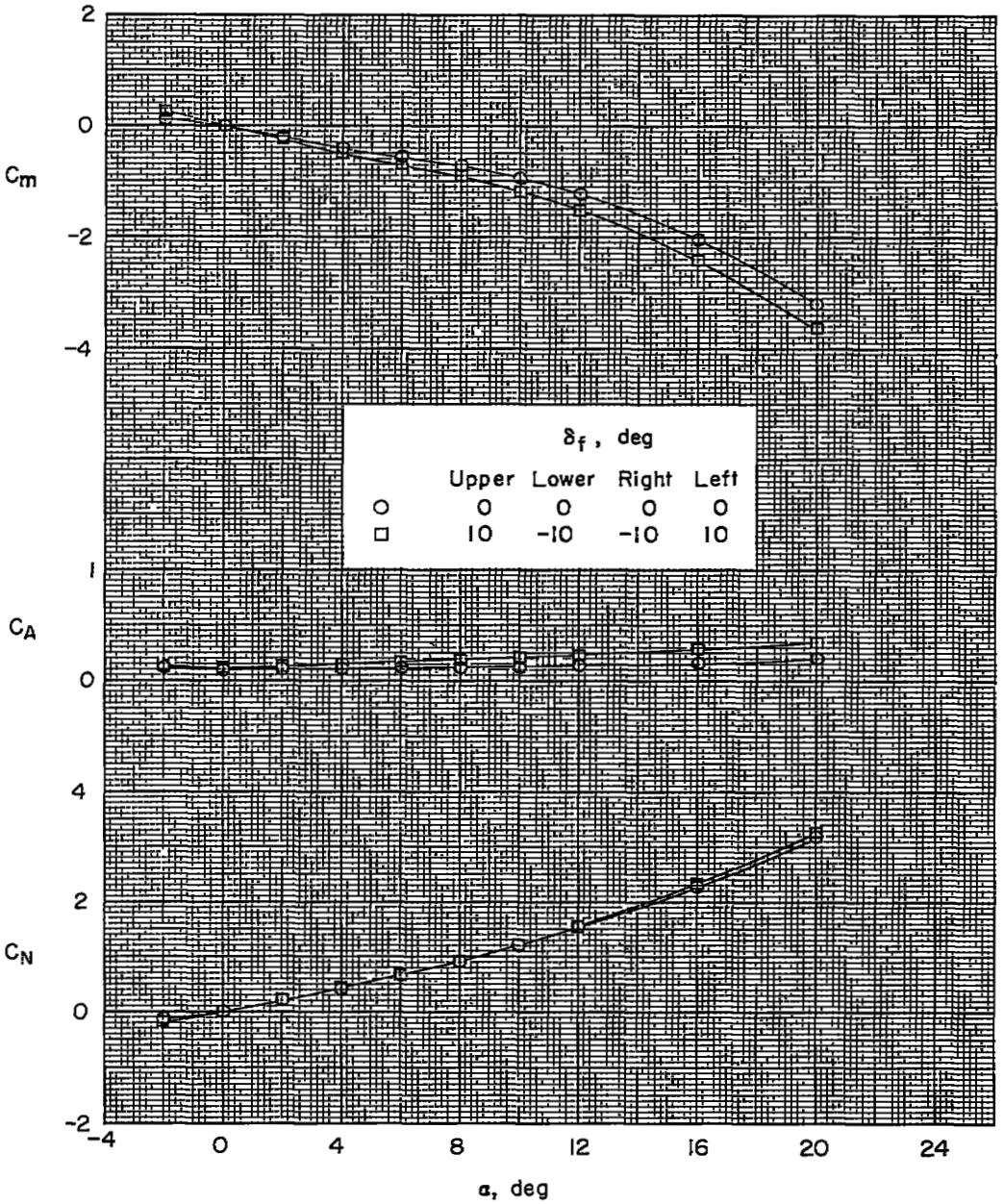

(b) Variation of C_m, C_A, and C_N with α.

Figure 6.- Concluded.

[redacted]

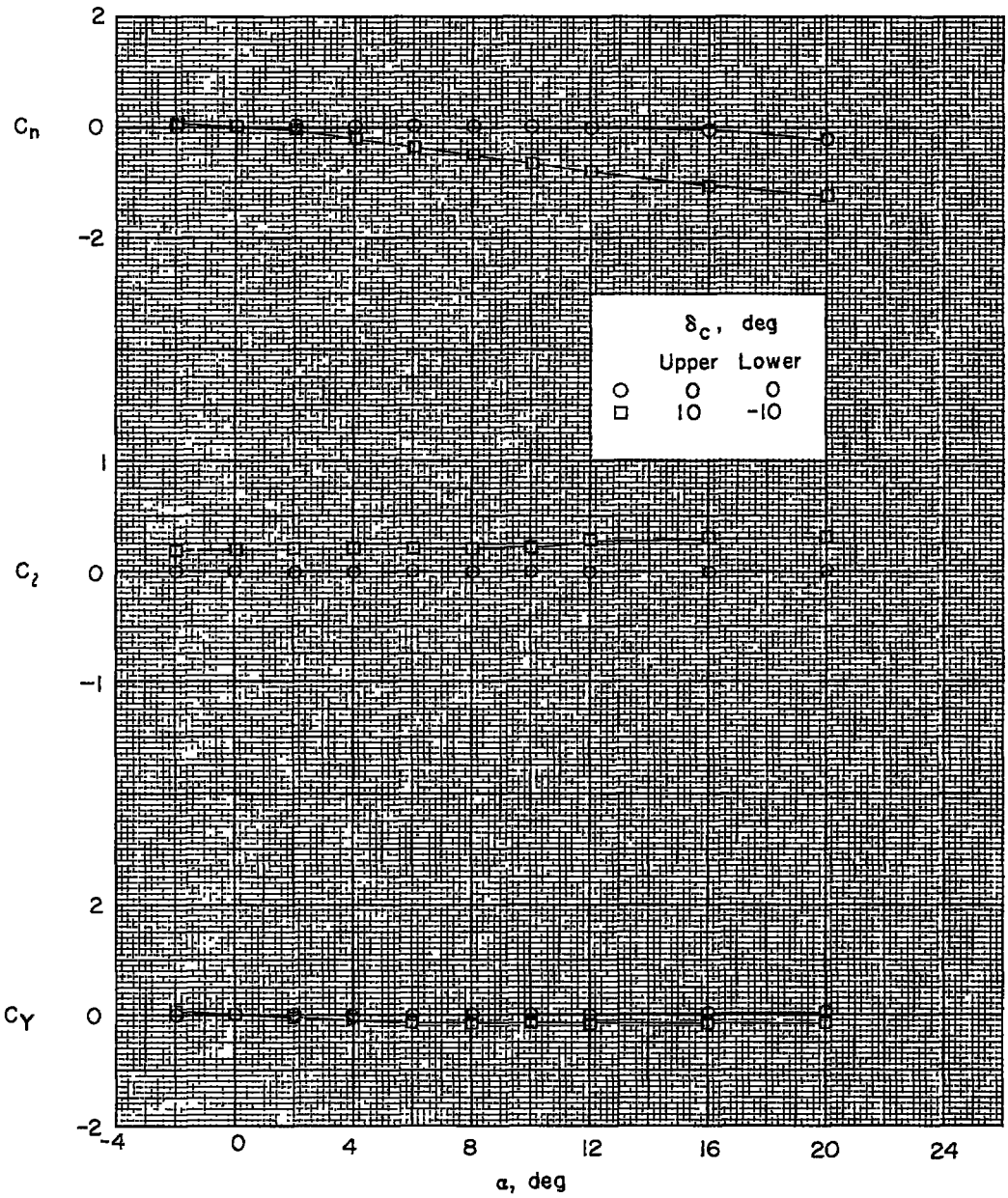

(a) Variation of C_n, C_l, and C_Y with α.

Figure 7.- Effects of differential deflection for roll control. Body with flare and all-movable control; horizontal controls at zero deflection; body-axis system.

[redacted]

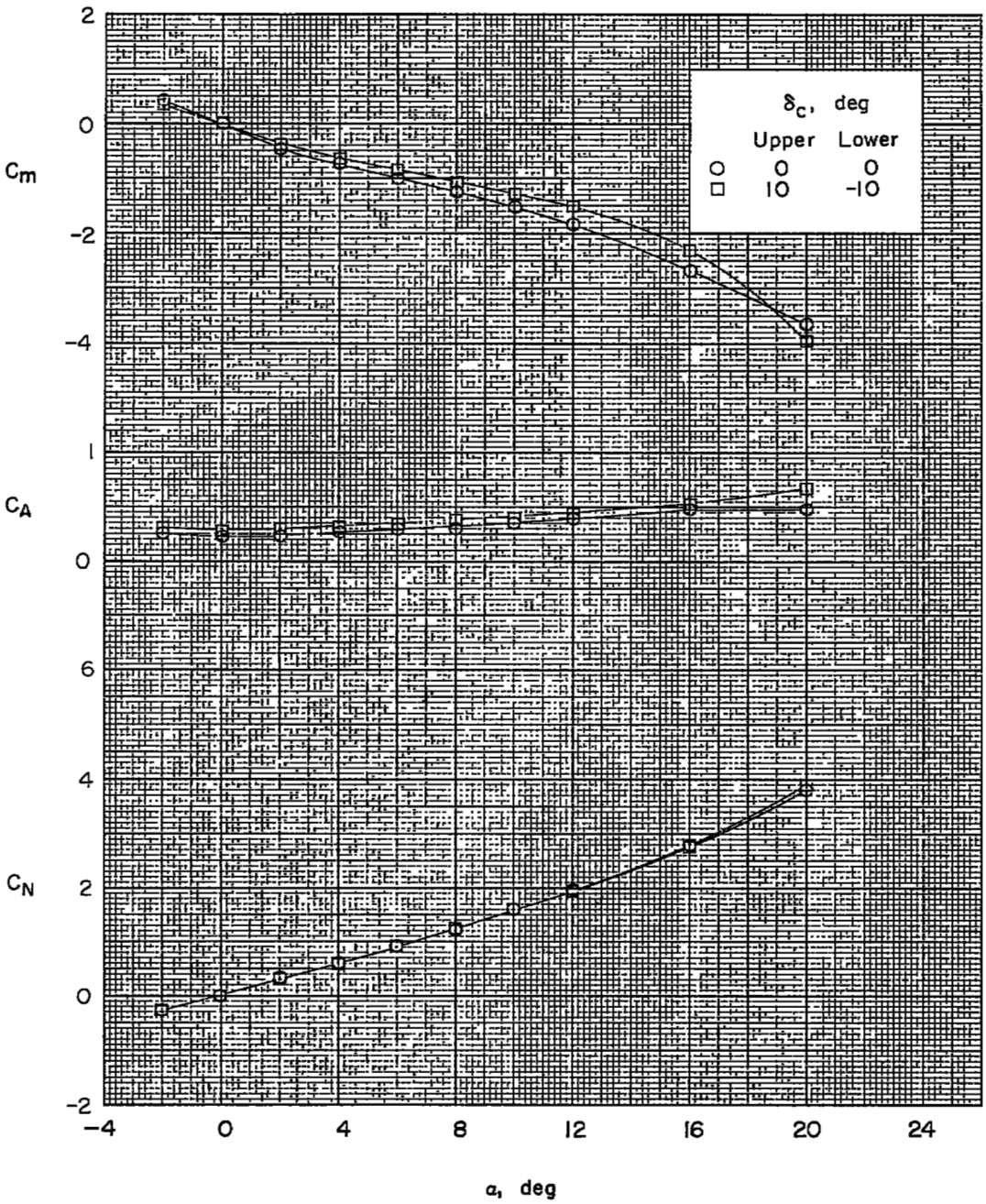

(b) Variation of C_m, C_A, and C_N with α.

Figure 7.- Concluded.